PCCP

Accepted Manuscript

ROYAL SOCIETY OF CHEMISTRY

www.rsc.org/pccp

Journal Name

RSCPublishing

ARTICLE

Complex Transition Metal Hydrides Incorporating Ionic Hydrogen: Thermal decomposition pathway of $Na_2Mg_2FeH_8$ and $Na_2Mg_2RuH_8$

Cite this: DOI: 10.1039/xoxxoooooox

Received ooth January 2012,
Accepted ooth January 2012

DOI: 10.1039/xoxxoooooox

www.rsc.org/

T. D. Humphries,[a]* M. Matsuo,[b] G. Li[a] and S. Orimo [a,b]

Complex transition metal hydrides have potential technological application as hydrogen storage materials, smart windows and sensors. Recent exploration of these materials has revealed that the incorporation of anionic hydrogen into these systems expands the potential number of viable complexes, while varying the countercation allows for optimisation of their thermodynamic stability. In this study, the optimised synthesis of $Na_2Mg_2TH_8$ (T = Fe, Ru) has been achieved and their thermal decomposition properties studied by ex situ Powder X-Ray Diffraction, Gas Chromatography and Pressure-Composition Isotherm measurements. The temperature and pathway of decomposition of these isostructural compounds differs considerably, with $Na_2Mg_2FeH_8$ proceeding via $NaMgH_3$ in a three-step process, while $Na_2Mg_2RuH_8$ decomposes via Mg_2RuH_4 in a two-step process. The first desorption maxima of $Na_2Mg_2FeH_8$ occurs at ca. 400 °C, while $Na_2Mg_2RuH_8$ has its first maxima at 420 °C. The enthalpy and entropy of desorption for $Na_2Mg_2TH_8$ (T = Fe, Ru) has been established by PCI measurements, with the ΔH_{des} for $Na_2Mg_2FeH_8$ being 94.5 kJ/mol H_2 and 125 kJ/mol H_2 for $Na_2Mg_2RuH_8$.

Introduction

Transition metals are renowned for their diverse range of valence states and structural conformations.[1,2] As such, in the last five decades a swathe of homoleptic transition metal hydrides have been synthesised to determine their potential for technological applications. Mg_2NiH_4 was first realised for its reversible hydrogenation properties in 1968,[3] and has since been investigated for a variety technological applications including smart windows and sensors.[4–7] Mg_2FeH_6, with a gravimetric hydrogen storage content of 5.5 wt% has since been developed,[8–14] along with a host of other transition metal hydride congeners and derivatives. [1,2,15–22]

The transition metal hydrides of Group 8 often form octahedral $[TH_6]^{4-}$ anions, of which are limited to four-fold coordination by counterions (M) in the form of $M^+M'^+M''^+M'''^+$, $M^{2+}M'^+M''^+$, $M^{3+}M'^+$, $M^{2+}M'^{2+}M''^+$. Expanding the diversity of coordination can be achieved by increasing the anionic charge of the system, for instance by the inclusion of H^-. A recent DFT study by Takagi et al. established that the incorporation of anionic hydrogen into complex transition metal hydride compounds enables inclusion of a wider variety of cations, thereby allowing tuning of these materials in order to optimise their thermodynamic properties or hydrogen storage capacities.[23] To date, a variety of quaternary complex hydrides have been synthesised and their structural and physical properties explored, these include $LaMg_2NiH_7$ ($La^{3+}\cdot 2Mg^{2+}\cdot 3H^-\cdot[NiH_4]^{4-}$),[18,24] $Na_2Mg_2NiH_6$ ($2Na^+\cdot 2Mg^{2+}\cdot 2H^-\cdot[NiH_4]^{4-}$),[25,19] $Na_2Mg_2TH_8$ ($2Na^+\cdot 2Mg^{2+}\cdot 2H^-\cdot[TH_6]^{4-}$) ($T$ = Fe, Ru),[20] MMg_2FeH_8 ($M^{2+}\cdot 2Mg^{2+}\cdot 2H^-\cdot[TH_6]^{4-}$) ($M$ = Ba, Ca, Sr; T = Fe, Ru, Os)[16,15,26] and $M_4Mg_4Fe_3H_{22}$ ($4Ca^{2+}\cdot 4Mg^{2+}\cdot 4H^-\cdot 3[FeH_6]^{4-}$) ($M$ = Ca, Yb).[27,28] Thermodynamic data for these materials are scarce, although some experimental[15,28] and DFT calculated[23] values have been determined. $SrMg_2FeH_8$ and $BaMg_2FeH_8$ decompose at *ca.* 440 and 450 °C under 0.1 MPa H_2,[15] respectively, while $Ca_4Mg_4Fe_3H_{22}$ and $Yb_4Mg_4Fe_3H_{22}$ decompose at *ca.* 395 and 420 °C,[28,27,1] respectively. The enthalpy of desorption of $Ca_4Mg_4Fe_3H_{22}$ and $Yb_4Mg_4Fe_3H_{22}$ to their corresponding binary hydrides has been calculated to be 122 and 137 kJ/mol H_2, respectively.[28] These values are significantly larger than those determined for the ternary Mg_2FeH_6 at 87 kJ/mol H_2,[29] which decomposes at *ca.* 300 °C,[13] and indicates the increased stabilisation offered by the incorporation of anionic hydrogen and varied cations into these quaternary compounds.

The isostructural compounds of $Na_2Mg_2FeH_8$ (5.1 wt% H) and $Na_2Mg_2RuH_8$ (4.0 wt% H) hold potential as hydrogen storage materials.[20] To make a fair assumption of their prospective

application, a true understanding of the physical properties of these novel quaternary complex transition metal hydrides must be determined, unto which the data is extremely sparse. As a consequence, the influence of H^- on the thermal stability and decomposition process of these materials is generally unknown and must be understood. As such, ex situ powder X-ray diffraction (PXD) and Pressure-Composition Isotherm Measurements (PCI) have been conducted. Their temperatures and pathways of decomposition have been established and the associated enthalpies and entropies of H_2 desorption have been calculated and compared to literature values.

Experimental

All preparation and manipulation was performed in a Miwa glove box filled with purified argon (<1 ppm O_2 and the dew point of H_2O below 190 K) to avoid contamination.

The synthesis of $Na_2Mg_2FeH_8$ was carried out by two methods:

S1 followed a four step process, which first required the synthesis of Mg_2FeH_6. This was achieved by mechanically milling (Fritsch Pulverisette 7) MgH_2 (hydrogen storage grade, Sigma Aldrich) and Fe (99.99%, Mitsuwa) powders at a molar ratio of 2:1 for 2 h at 400 rpm (ball-to-powder ratio 40:1), under argon with subsequent heat treatment of the pelletised powder at 400 °C for 20 h under 3 MPa H_2. The resultant olive green powder was then mechanically milled with NaH (95 %, Sigma Aldrich) at a molar ratio of 1:2 for 20 h under argon (S1-BM) with subsequent heat treatment of the pelletised powder at 400 °C for 20 h under 30 MPa H_2. The product was yielded as an olive green powder.

The synthesis of **S2** ($Na_2Mg_2FeH_8$) followed a two-step process. NaH, MgH_2 and Fe powders at a molar ratio of 2:2:1 were mechanically milled for 20 h at 400 rpm (ball-to-powder ratio 40:1), under argon (S2-BM) with subsequent heat treatment of the pelletised powder at 400 °C for 60 h under 30 MPa H_2. The product was yielded as an olive green powder.

The synthesis of $Na_2Mg_2RuH_8$ followed a two-step process. MgH_2, NaH and Ru (99.9 %, Kojundo Chemical Laboratory) were mechanically milled (identical parameters as employed with $Na_2Mg_2FeH_8$) at a molar ratio of 2:2:1 for 20 h under argon (S3-BM), before subsequent heat treatment of the pelletised powder at 500 °C for 20 h under 30 MPa H_2. The product was yielded as a light grey powder.

Powder X-ray diffraction (PXD) measurements were conducted using a conventional X-ray diffractometer (Lab-PXD, PANalytical X'Pert-Pro, CuKα radiation) in flat plate mode. Data were collected using a X'Celerator X linear position sensitive detector within a 2θ range of 10 - 90° using 0.02° steps at 0.04 °/s with the X-ray generator operating conditions of 45 kV and 40 mA. The PXD samples were loaded in an Ar glovebox and the sample holder covered by Mylar film to prevent oxygen/moisture contamination during data collection. PANalytical HighScore Plus v. 3.0, DICVOL,[30] CHEKCELL[31] and GSAS[32,33] were used for phase identification, indexing, space group identification and Rietveld refinement, respectively.

A GC323 (Gas Chromatography) (GL sciences Inc.) was used to detect the desorbed H_2 by means of a TCD detector, with a column temperature of 200 °C. Samples were heated at a rate of 5 °C/min under an Ar flow of 40 ml/min.

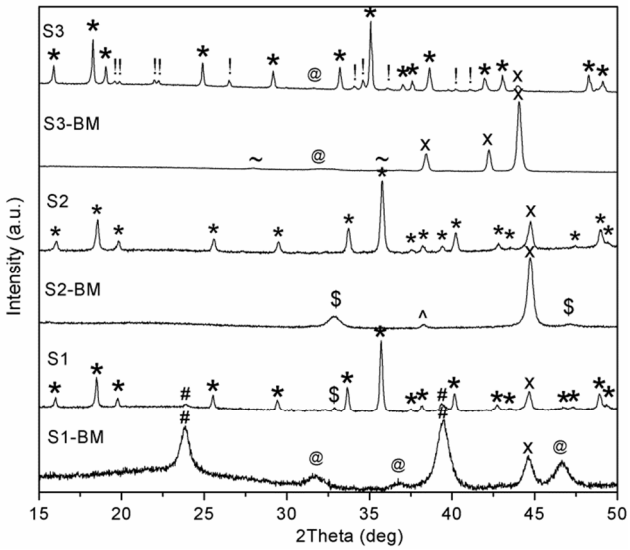

Figure 1. PXD of ball milled samples S1-BM (Mg_2FeH_6 + 2NaH), S2-BM (2NaH + $2MgH_2$ + Fe) and S3-BM ($2MgH_2$ + 2NaH + Ru) and hydrogenated samples of S1-3. λ = CuKα. * = $Na_2Mg_2TH_8$ (*T* = Fe, Ru); # = Mg_2FeH_6; @ = NaH; x = *T* (Fe, Ru); $ = $NaMgH_3$; ^ = NaOH; + = Mg; ~ MgH_2; ! = unknown phase.

Typical Pressure-Composition Isotherm Measurements (PCI) were conducted inside custom-built manometric apparatus, where the sample cell was placed in a furnace and heated to the desired temperature at a hydrogen pressure of 6 MPa or 30 MPa. The experiment was controlled by software developed by Suzuki Shokan Co., Ltd.

Results and Discussion

Synthesis of $Na_2Mg_2TH_8$ (*T* = Fe, Ru)

The synthesis of $Na_2Mg_2FeH_8$ was first reported to utilise Mg_2FeH_6 as a starting material, which was consequently milled for 20 h with NaH (S1-BM), followed by hydrogenation at 30 MPa H_2 at 400 °C (Eqs 1 and 2).[20] Overall, this method is time intensive (in excess of 100 h due to the requirement of two milling and two hydrogenation procedures), and the final product also contains Fe, NaH, and Mg_2FeH_6 impurities. In order to reduce the time requirements and levels of impurities, alternative synthetic routes were investigated. It was determined that successful synthesis is achievable by ball milling 2NaH + MgH_2 + Fe (S2-BM), followed by hydrogenation at 30 MPa H_2 at 400 °C (Eq. 3), with an associated time requirement of 80 h. The products after milling of each material differ considerably (Figure 1), the constituents of S1-BM, identified by PXD are not altered during milling

(Mg_2FeH_6 + NaH) despite a broadening of the peaks due to a decrease of crystallite size (or reduced crystallinity).[34] The products of S2-BM were $NaMgH_3$ + Fe.[35]

Hydrogenation of the ball milled samples S1-BM and S2-BM under standard conditions (30 MPa H_2 and 400 °C for 60 h), resulted in the formation of $Na_2Mg_2FeH_8$ as the major phase (Figure 1). Analysis of hydrogenated S1 by Reitveld refinement indicates that the sample is 80.3(9) % pure and as such contains residual Mg_2FeH_6 (8.9(4) %), Fe (7.9(2) %), $NaMgH_3$ (2.5(3) %) and NaH (2.7(2) %) starting materials. Analysis of hydrogenated S2 indicates that the sample contains 90.6(4) % $Na_2Mg_2FeH_8$ and 9.4(3) % Fe, without residual Mg_2FeH_6 or NaH. This indicates that the optimal method of synthesis is via the S2 method due to the elimination of the prerequisite Mg_2FeH_6 synthesis (Eq. 1) and overall decrease in impurities compared to S1, primarily due to the initial (complete) formation of $NaMgH_3$ during the milling reaction. Milling initiates the breaking of the strong Na-H bonds, which is required to ensue during the annealing phase when synthesised via Mg_2FeH_6 (S1). This ultimately leads to the observation of unreacted NaH and Mg_2FeH_6 starting materials.

The synthesis of $Na_2Mg_2RuH_8$ follows a two-step reaction, where stoichiometric quantities of Ru, NaH and MgH_2 are

$$2MgH_2 + Fe \xrightarrow[(2)\ 3\ MPa\ H_2,\ 400\ °C,\ 20\ h]{(1)\ 2\ h\ BM} Mg_2FeH_6 \quad (1)$$

$$Mg_2FeH_6 + 2NaH \xrightarrow[(2)\ 30\ MPa\ H_2,\ 400\ °C,\ 60\ h]{(1)\ 20\ h\ BM} Na_2Mg_2FeH_8 \quad (2)$$

$$2MgH_2 + 2NaH + Fe \xrightarrow[(2)\ 30\ MPa\ H_2,\ 400\ °C,\ 60\ h]{(1)\ 20\ h\ BM} Na_2Mg_2FeH_8 \quad (3)$$

milled for 5 h (S3-BM) before hydrogenation under 30 MPa H_2 at 500 °C for 20 h (S3) (Eq.4).[20] The composition of the milled material is unchanged from the starting materials (Figure 1), whereas after hydrogenation the sample appears to be mostly $Na_2Mg_2RuH_8$, but also comprises of some residual Ru. An unknown material is also identifiable within the $Na_2Mg_2RuH_8$ powder (S3), of which only a few reflections are discernible. These occurrence of these additional Bragg peaks were also noted previously.[20]

$$2NaH + 2MgH_2 + Ru \xrightarrow[(2)\ 30\ MPa\ H_2,\ 500\ °C,\ 20\ h]{(1)\ 5\ h\ BM} Na_2Mg_2RuH_8 \quad (4)$$

Thermal Decomposition of $Na_2Mg_2TH_8$ (T = Fe, Ru)

In order to determine the thermal decomposition temperatures of $Na_2Mg_2TH_8$ (T = Fe, Ru), aliquots of each material were heated at a rate of 5 °C/min with GC detecting the

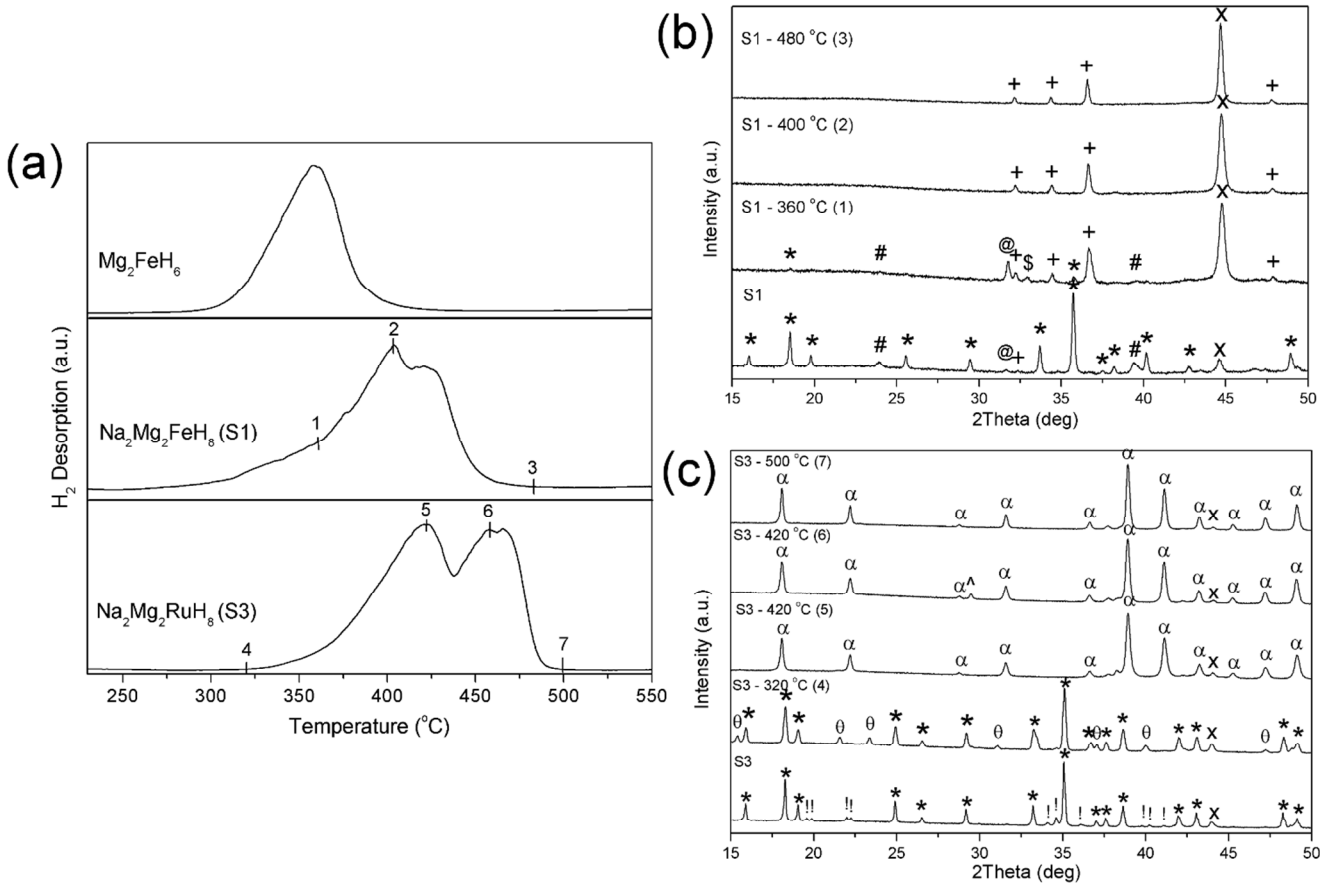

Figure 2. (a) GC analysis of Mg_2FeH_6, $Na_2Mg_2FeH_8$ (S1) and $Na_2Mg_2RuH_8$ (S3) (ΔT = 5 °C/min). *Ex situ* PXD analysis of (b) $Na_2Mg_2FeH_8$ (S1) and (c) $Na_2Mg_2RuH_8$ (S3) at selected temperatures (λ = CuKα). Numbers on GC plots correlate to temperatures at which samples were heated prior to PXD analysis. * = $Na_2Mg_2TH_8$ (T = Fe, Ru); # = Mg_2FeH_6; @ = NaH; x = T (Fe, Ru); $ = $NaMgH_3$; ^ = NaOH; + = Mg; α = Mg_3Ru_2; ! = unknown phase; θ = unknown phase.

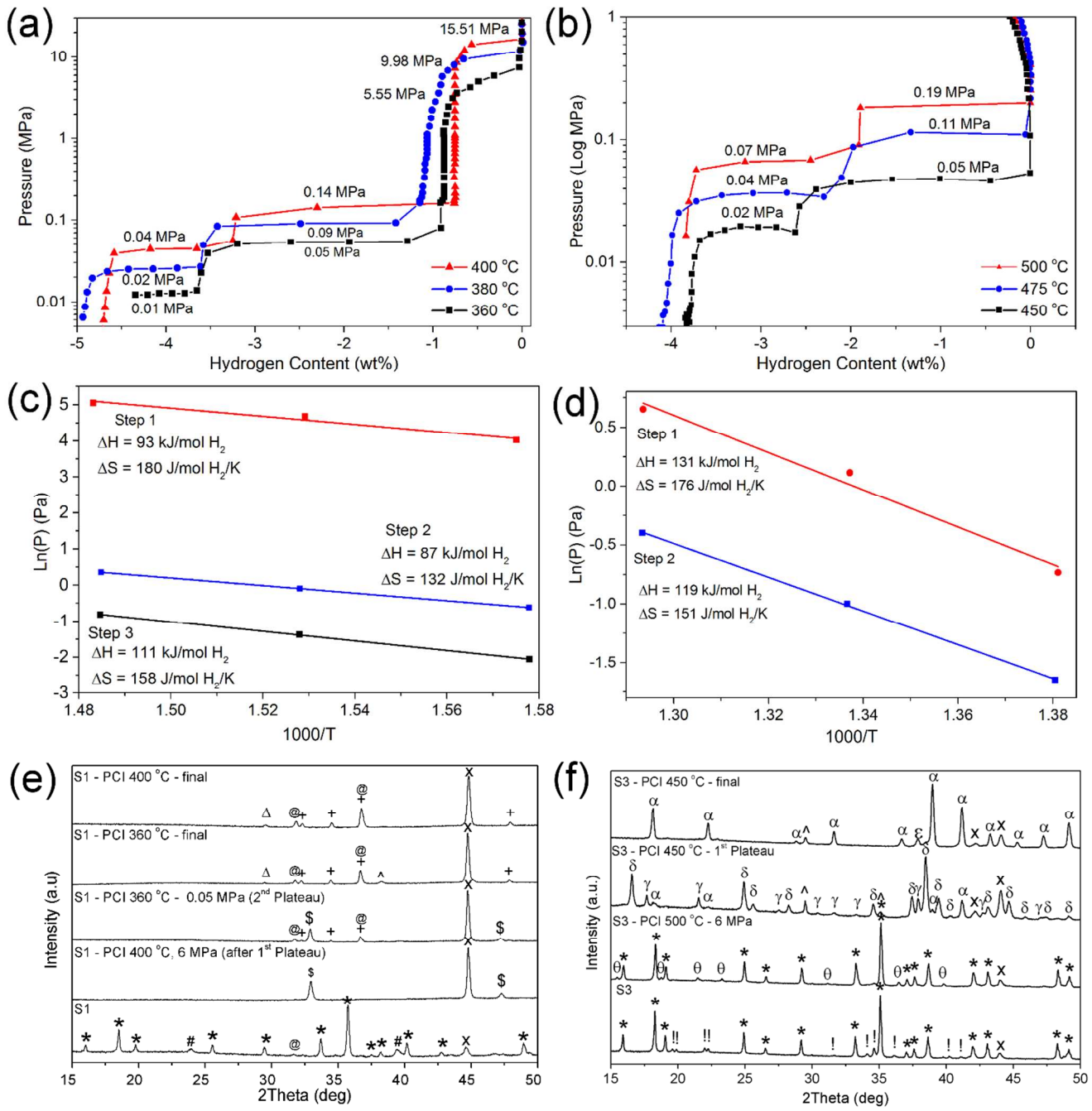

Figure 3. PCI analysis of $Na_2Mg_2FeH_8$ (a) and $Na_2Mg_2RuH_8$ (b) at selected temperatures. van't Hoff plot of H_2 desorption equilibrium pressures and the linear fit to the data for $Na_2Mg_2FeH_8$ (c) and $Na_2Mg_2RuH_8$ (d). *Ex situ* PXD analysis of $Na_2Mg_2FeH_8$ (S1) (e) and $Na_2Mg_2RuH_8$ (S3) (f) for samples collected after PCI analysis and after rehydrogenation (λ = CuKα). * = $Na_2Mg_2TH_8$ (*T* = Fe, Ru); # = Mg_2FeH_6; @ = NaH; x = *T* (Fe, Ru); $ = $NaMgH_3$; ^ = NaOH; + = Mg; Δ = Na; α = Mg_3Ru_2; δ = Mg_2RuH_4; ! = unknown phase; θ = unknown phase; γ = unknown phase; ε = unknown phase.

corresponding desorbed H_2. The chromatograms obtained (Figure 2a) are similar, with two stages of H_2 desorption being observed for both materials (S1 and S3). The onset of decomposition for $Na_2Mg_2FeH_8$ occurs at *ca.* 280 °C, with the first maxima being observed at ca. 400 °C, and the second at ca. 430 °C. Decomposition concludes at *ca.* 475°C. Conversely, the onset of H_2 desorption for $Na_2Mg_2RuH_8$ occurs at *ca.* 325 °C, with the first maxima being observed at *ca.* 421 °C, and the second at ca. 460 °C. H_2 is no longer detected after *ca.* 500 °C.

To ascertain the pathway of decomposition, *ex situ* PXD was conducted on samples heated to selected temperatures *in vacuo* (Figures 2b and c). Analysis of $Na_2Mg_2FeH_8$ after heating at 360 °C indicates a miniscule quantity of $Na_2Mg_2FeH_8$ resides, although the majority has decomposed into NaH, Mg and Fe,

while $NaMgH_3$ is also detected. By 400 °C NaH has decomposed, while only Mg and Fe are observable by PXD. Na is not observed due to the low vapor pressure of Na at elevated temperatures. No further changes to the material are observed at higher temperatures. Therefore the decomposition of $Na_2Mg_2FeH_8$ is determined to occur according to Eqs. 5-7.

$$Na_2Mg_2FeH_8 \rightarrow 2NaMgH_3 + Fe + H_2 \quad (1.3\ wt\%) \quad (5)$$

$$2NaMgH_3 + Fe \rightarrow 2NaH + 2Mg + 2H_2 + Fe \quad (2.5\ wt\%) \quad (6)$$

$$2NaH + 2Mg + Fe \rightarrow 2Na + 2Mg + Fe + H_2 \quad (1.3\ wt\%) \quad (7)$$

$Na_2Mg_2RuH_8$ was first heated to 320 °C, where PXD determined that decomposition has not yet started. By 420 °C full decomposition appears to be complete, with Mg_3Ru_2 and Ru being the products. At this temperature, NaH instantly decomposes to Na and evaporates from the sample. As a result, the decomposition of $Na_2Mg_2RuH_8$ is determined to occur according to Eqs. 8 and 9. Presumably the excess Ru required to form Mg_3Ru_2 (without leaving excess Mg) comes from the excess Ru that remained in the starting material.

$$Na_2Mg_2RuH_8 \rightarrow 2NaH + \tfrac{2}{3}Mg_3Ru_2 + 3H_2 \quad (3.0\ wt\%) \quad (8)$$

$$2NaH + Mg_3Ru_2 \rightarrow 2Na + Mg_3Ru_2 + H_2 \quad (1.0\ wt\%) \quad (9)$$

PCI analysis of $Na_2Mg_2TH_8$ (T = Fe, Ru) (Figures 3a and b) enables the intricacies of the decomposition process to be truly understood. The experiments on $Na_2Mg_2FeH_8$ were conducted at initial pressures of 30 MPa and 400 °C, mimicking conditions used for synthesis. Consequently, it was ascertained that the first thermal reaction according to Eq. 5, occurs at an equilibrium pressure of 15.5 MPa, releasing ca. 0.8 wt% H_2 at 400 °C (Figure 4a). PXD analysis of the products recovered at 6 MPa characterised the products to be $NaMgH_3$ and Fe (Figure 3e). ΔH_{dec} for this process was determined by means of a van't Hoff plot of H_2 desorption equilibrium pressures and the linear fit (R^2 = 0.975) to the data to be 93 kJ/mol H_2 (Figure 3c), while the corresponding ΔS_{dec} was calculated as 180 J/mol H_2/K. However, at lower temperatures this step is kinetically hindered and as a result ΔH and ΔS may be obscured. The values reported above are an average of the plateau pressures.

The further two equilibrium plateaus below 1 MPa H_2 correspond to the decomposition of $NaMgH_3$, exhibiting mass losses of 2.5 and 1.5 wt% for Eqs. 6 and 7, respectively. The overall hydrogen content released was therefore determined to be 4.7 wt% at 400 °C (theoretical maximum of 5.1 wt%). ΔH_{dec} was calculated to be 87 and 111 kJ/mol H_2 for the latter two processes, in accord with the literature values.[36] The corresponding ΔS_{dec} also agreed with literature values with 132 and 158 J/mol H_2/K for Eq. 6 and 7, respectively. Therefore ΔH_{des} for the entire system is surmised to be 378 kJ/mol (94.5 kJ/mol H_2). The identity of the species at each decomposition stage was determined by PXD by ending selected PCI experiments at specified pressures. Figure 3e illustrates the final products after the PCI experiments conducted at 360 and 400 °C and also those observed after the first and during the

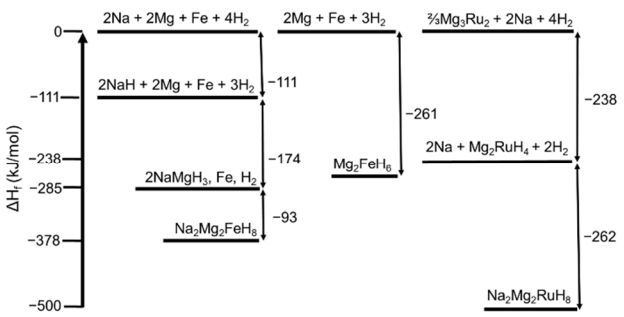

Figure 4. Energy diagram illustrating the experimentally determined enthalpies of formation (ΔH_{form} kJ/mol) of $Na_2Mg_2FeH_8$, Mg_2FeH_6,[29] and $Na_2Mg_2RuH_8$. The excess Ru required to form Mg_3Ru_2 is acquired from the impurity Ru remaining in the $Na_2Mg_2RuH_8$ starting material.

second equilibrium step (Eq. 6). During the second equilibrium step, $NaMgH_3$, Fe and NaH, and Mg are observed, indicating that $NaMgH_3$ is decomposing. After the third equilibrium (final products), Na, Mg and Fe are the main constituents, although residual NaH is also observed. Therefore the decomposition process can be described according to Eqs. 5-7 and Figure 4.

The thermal stability of $Na_2Mg_2FeH_8$ is enhanced compared to that of Mg_2FeH_6, which exhibits a H_2 desorption maxima at *ca.* 360 °C (Figure 2) with an associated ΔH_{des} of 261 kJ/mol.[29] The additional stability achieved by the incorporation of Na^+ and H^- into the compound, induces a significant increase in desorption temperature maxima to 400°C and a total ΔH_{des} of 378 kJ/mol (Figure 4). This value correlates very well with the previous DFT calculations conducted on this compound, which determined ΔH_f to be −328 kJ/mol.[23]

In contrast to $Na_2Mg_2FeH_8$, $Na_2Mg_2RuH_8$ is stable above pressures of 0.19 MPa H_2 and T >500°C (Figure 3a). PXD analysis of material annealed at 6 MPa H_2 and 450 °C (Figure 3f) indicates that the only modification is the disappearance of the unknown phase (observed after initial synthesis (Figure 1)) which is replaced by another unknown phase. This material can be indexed to an orthorhombic unit cell of a = 14.5331, b = 7.9841 and c = 6.2429 and crystallises in a possible space group of *Pmmn*, although structural identification is inhibited by the low concentration and weak intensity of the Bragg peaks. As was observed from the GC results (Figure 1), decomposition is also noted to follow a two-step decomposition route by PCI. At 500 °C, the first plateau is observed at an equilibrium pressure of 0.19 MPa, while the second occurs at ca. 0.07 MPa. Each step was determined to have an associated mass loss of ca. 1.9 wt%, with a total of 3.8 wt% H_2 being desorbed out of a maximum theoretical capacity of 4.0 wt%. This process was also carried out at 475 and 450 °C. This allowed for ΔH_{des} and ΔS to be determined to be 131 kJ/mol H_2 and 176 ΔS (J/mol H_2/K), respectively for step 1 (R^2 = 0.984) and ΔH_{des} = 119 kJ/mol H_2 and ΔS = 151 ΔS (J/mol H_2/K) for step 2 (R^2 = 0.999) (Figure 3d). Therefore ΔH_{des} for the entire system is surmised to be 500 kJ/mol (125 kJ/mol H_2). PXD of the products at each stage allows a greater insight into those determined by *ex situ* heating *in vacuo*. After the first plateau, a substantial level of Mg_2RuH_4 is identifiable in the powder,

along with Ru, NaOH and a small quantity of Mg_3Ru_2. The highly oxidisable Na (residual after evaporation) is the source of NaOH (occurring during PXD analysis), while the thermally unstable Mg_2RuH_4 is the source of Mg_3Ru_2. An unknown phase is also observed at this temperature and pressure, which due to the low intensity of the Bragg peaks associated with this material, indexing and as such, structural refinement was not possible. After the second plateau, the remaining powder consists of Mg_3Ru_2 and Ru. Presumably the excess Ru required to form Mg_3Ru_2 (without leaving excess Mg) comes from the excess Ru that remains in the starting material (Figure 1). Therefore the decomposition process can be described according to Eqs. 10 and 11 and Fig. 4.

$$Na_2Mg_2RuH_8 \rightarrow 2Na + Mg_2RuH_4 + 2H_2 \quad (2.0\ wt.\%\ H_2) \quad (10)$$

$$Mg_2RuH_4 + 2Na \rightarrow Mg_3Ru_2 + 2Na + 2H_2 \quad (2.0\ wt.\%\ H_2) \quad (11)$$

The decomposition pathway of these materials differ significantly in that $NaMgH_3$ is the intermediate for $Na_2Mg_2FeH_8$, while $Na_2Mg_2RuH_8$ disassembles via Mg_2RuH_4 (Figure 4). The versatile 4*d* Ru metal center is known to form a variety of complex anions including $[Ru_2H_6]^{12-}$, $[RuH_4]_n^{4n-}$, $[RuH_5]_{av}^{5-}$, $[RuH_6]^{4-}$ and $[RuH_7]^{3-}$, while the 3*d* Fe metal center is only known to form $[FeH_6]^{4-}$ anions.[1] As a consequence, $Na_2Mg_2RuH_8$ forms the $[RuH_4]_n^{4n-}$ polyanionic intermediate upon decomposition,[37] whereas $Na_2Mg_2FeH_8$ preferentially decomposes to the thermally stable $NaMgH_3$[36] rather than Mg_2FeH_6 (Figure 4). Mg_2RuH_4 was not observed during the *ex situ* heating experiments of $Na_2Mg_2RuH_8$ (Figure 2e)as it is not thermodynamically stable at the temperatures at which $Na_2Mg_2RuH_8$ decomposes (420 °C, *in vacuo*).[37] Although, the synthesis of Mg_2RuH_4 is accomplished at 450 °C under 0.2 MPa H_2, it would presumably decompose at the temperatures imposed here, especially *in vacuo*. Stabilisation of this species is therefore viable under H_2 pressures of 0.05 – 0.02 MPa.

Conclusions

The optimised syntheses of $Na_2Mg_2TH_8$ (T = Fe, Ru) have been reported. Ball milling of stoichiometric quantities of NaH, MgH_2 and Fe followed by hydrogenation allows for a yield of >90 % purity of $Na_2Mg_2FeH_8$ via the formation of a $NaMgH_3$ intermediate. On the contrary, no intermediate is observed during the synthesis of $Na_2Mg_2RuH_8$ using an identical procedure.

The thermal decomposition of both $Na_2Mg_2TH_8$ materials have been studied by *ex situ* PXD, GC and PCI measurements. The first desorption maxima of $Na_2Mg_2FeH_8$ has been established to occur at *ca.* 400 °C, while $Na_2Mg_2RuH_8$ has its first maxima at 420 °C. The decomposition pathways of these isostructural compounds differs considerably, with $Na_2Mg_2FeH_8$ proceeding via $NaMgH_3$ in a three-step process, while $Na_2Mg_2RuH_8$ decomposes via Mg_2RuH_4 in a two-step process. The dissimilarity between the pathways originates from the capability of the 4*d* Ru metal centre to exist in a variety of $[RuH_x]^{n-}$ complexes compared to Fe, which only exists as $[FeH_6]^{4-}$.

The enthalpy and entropy of desorption for $Na_2Mg_2TH_8$ (T = Fe, Ru) for each stage of decomposition has been established to be by PCI measurements. The total enthalpy of desorption for $Na_2Mg_2FeH_8$ is 94.5 kJ/mol H_2 and 125 kJ/mol H_2 for $Na_2Mg_2RuH_8$.

Acknowledgements

We would like to acknowledge Ms. Warifune for the synthesis of the Mg_2FeH_6 starting material. We also appreciate the financial support from JSPS KAKENHI Grant Number 25220911.

Notes and references

[a] WPI-Advanced Institute for Materials Research, Tohoku University, 2-1-1 Katahira, Aoba-ku, Sendai 980-8577, Japan. Fax: +81-22-215-2091; Tel.: +81-22-215-2094; E-mail: terry_humphries81@hotmail.com.

[b] Institute for Materials Research, Tohoku University, 2-1-1 Katahira, Aoba-ku, Sendai 980-8577, Japan. Fax: +81-22-215-2091; Tel.: +81-22-215-2093; E-mail: orimo@imr.tohoku.ac.jp.

1. K. Yvon and G. Renaudin, in *Encyclopedia of Inorganic Chemistry*, John Wiley & Sons, Ltd, 2006.
2. K. Yvon, *Chimia (Aarau).*, 1998, **52**, 613–619.
3. J. J. Reilly and R. H. Wiswall, *Inorg. Chem.*, 1968, **7**, 2254–2256.
4. H. Blomqvist and D. Noréus, *J. Appl. Phys.*, 2002, **91**, 5141–5148.
5. M. Lelis, D. Milcius, E. Wirth, U. Halenius, L. Eriksson, K. Jansson, K. Kadir, J. Ruan, T. Sato, T. Yokosawa, and D. Noréus, *J. Alloys Compd.*, 2010, **496**, 81–86.
6. R. J. Westerwaal, M. Slaman, C. P. Broedersz, D. M. Borsa, B. Dam, R. Griessen, A. Borgschulte, W. Lohstroh, B. Kooi, G. ten Brink, K. G. Tschersich, and H. P. Fleischhauer, *J. Appl. Phys.*, 2006, **100**, 063518.
7. T. J. Richardson, J. L. Slack, R. D. Armitage, R. Kostecki, B. Farangis, and M. D. Rubin, *Appl. Phys. Lett.*, 2001, **78**, 3047–3049.
8. M. Polanski, T. K. Nielsen, Y. Cerenius, J. Bystrzycki, and T. R. Jensen, *Int. J. Hydrogen Energy*, 2010, **35**, 3578–3582.
9. M. Polanski, K. Witek, T. K. Nielsen, L. Jaroszewicz, and J. Bystrzycki, *Int. J. Hydrogen Energy*, 2013, **38**, 2785–2789.
10. J. J. Didisheim, P. Zolliker, K. Yvon, P. Fischer, J. Schefer, M. Gubelmann, and A. F. Williams, *Inorg. Chem.*, 1984, **23**, 1953–1957.
11. G. Li, M. Matsuo, S. Deledda, R. Sato, B. C. Hauback, and S. Orimo, *Mater. Trans.*, 2013, **54**, 1532–1534.
12. T. J. Richardson, J. L. Slack, B. Farangis, and M. D. Rubin, *Appl. Phys. Lett.*, 2002, **80**, 1349–1351.
13. B. Bogdanović, A. Reiser, K. Schlichte, B. Spliethoff, and B. Tesche, *J. Alloys Compd.*, 2002, **345**, 77–89.
14. S. F. Parker, K. P. J. Williams, M. Bortz, and K. Yvon, *Inorg. Chem.*, 1997, **36**, 5218–5221.
15. B. Huang, K. Yvon, and P. Fischer, *J. Alloys Compd.*, 1995, **227**, 121–124.
16. B. Huang, F. Gingl, F. Fauth, A. Hewat, and K. Yvon, *J. Alloys Compd.*, 1997, **248**, 13–17.
17. B. Huang, K. Yvon, and P. Fischer, *J. Alloys Compd.*, 1994, **204**, 5–8.

18. G. Renaudin, L. Guenee, and K. Yvon, *J. Alloys Compd.*, 2003, **350**, 145–150.
19. M. Orlova, J.-P. Rapin, and K. Yvon, *Inorg. Chem.*, 2009, **48**, 5052–5054.
20. T. D. Humphries, S. Takagi, G. Li, M. Matsuo, T. Sato, M. H. Sørby, S. Deledda, B. C. Hauback, and S. Orimo, *J. Alloys Compd.*, 2015, doi:10.1016/j.jallcom.2014.12.113.
21. M. Matsuo, H. Saitoh, A. Machida, R. Sato, S. Takagi, K. Miwa, T. Watanuki, Y. Katayama, K. Aoki, and S. Orimo, *RSC Adv.*, 2013, **3**, 1013–1016.
22. H. Saitoh, S. Takagi, M. Matsuo, Y. Iijima, N. Endo, K. Aoki, and S. Orimo, *APL Mat.*, 2014, **2**, 076103.
23. S. Takagi, T. D. Humphries, K. Miwa, and S. Orimo, *Appl. Phys. Lett.*, 2014, **104**, 203901.
24. M. Di Chio, L. Schiffini, S. Enzo, G. Cocco, and M. Baricco, *J. Alloys Compd.*, 2007, **434**, 734–737.
25. K. Kadir and D. Noréus, *Inorg. Chem.*, 2007, **46**, 3288–3289.
26. B. Huang, K. Yvon, and P. Fischer, *J. Alloys Compd.*, 1992, **187**, 227–232.
27. B. Huang, K. Yvon, and P. Fischer, *J. Alloys Compd.*, 1992, **190**, 65–68.
28. B. Huang, K. Yvon, and P. Fischer, *J. Alloys Compd.*, 1993, **197**, 65–68.
29. J. A. Puszkiel, P. Arneodo Larochette, and F. C. Gennari, *J. Alloys Compd.*, 2008, **463**, 134–142.
30. A. Boultif and D. Louer, *J. Appl. Crystallogr.*, 2004, **37**, 724–731.
31. J. Laugier and B. Bochu, *LMGP-Suite Suite Programs Interpret. X-ray Exp. by Jean laugier Bernard Bochu, ENSP/Laboratoire des Matériaux du Génie Phys. BP 46. 38042 Saint Martin d'Hères, Fr.*
32. B. H. Toby, *J. Appl. Crystallogr.*, 2001, **34**, 210–213.
33. A. C. Larson and R. B. Von Dreele, *Los Alamos Natl. Lab. Rep. LAUR*, 2000, 86–748.
34. B. E. Warren, *X-ray Diffraction*, Courier Dover Publications, 1969.
35. H. Reardon, N. Mazur, and D. H. Gregory, *Prog. Nat. Sci. Mater. Int.*, 2013, **23**, 343–350.
36. D. A. Sheppard, M. Paskevicius, and C. E. Buckley, *Chem. Mater.*, 2011, **23**, 4298–4300.
37. F. Bonhomme, K. Yvon, G. Triscone, K. Jansen, G. Auffermann, P. Müller, W. Bronger, and P. Fischer, *J. Alloys Compd.*, 1992, **178**, 161–166.